9-2023

A Hybrid Class Autonomous Underwater Vehicle

Tyler J. Inkley

A Hybrid Class Autonomous Underwater Vehicle

Link Foundation Fellowship Report

Tyler J. Inkley
University of Hawai'i at Mānoa
Ocean Engineering and Instrumentation Fellowship 2022

Prepared for: Dr. Javad Hashemi

September 1, 2023

I Project Narrative

I.i Introduction

I.i.a Background

Underwater robots can largely be classified into two distinct groups: underactuated Autonomous Underwater Vehicles (AUVs) with low-drag slender bodies for efficient long-range travel, and Remotely Operated Vehicles (ROVs) with numerous thrusters for accurate low-speed maneuverability at the expense of drag. Both distinctions present inherent limitations. AUVs possess inaccurate small-scale maneuvering, while ROVs are cumbersome and range limited, both of which require expensive manned infrastructure for operation. As underwater robots increasingly become indispensable oceanography instruments, the development of a next-generation vehicle without suffering these design trade-offs becomes paramount.

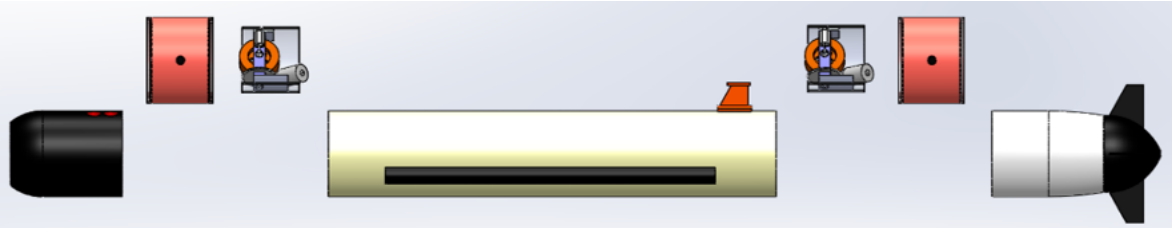

Figure 1: Proposed hybrid class AUV architecture - front view with additional actuation modules in streamlined hull form

A "hybrid class" AUV, capable of both efficient long-range travel and low-speed high-accuracy maneuvering would enhance performance allowing operation in previously inaccessible regions, and reducing the cost of an extended marine robot presence in the oceans. While bio-inspired thrusters have shown to provide maneuvering forces without compromising a streamlined body shape within a laboratory setting [1], for this vehicle to be utilized in remote locations it must have sophisticated control algorithms that can handle complex environments, and a sensory system that can adequately measure those surroundings to accompany improved maneuvering capabilities. This project sought to develop novel AUV technology that couples bio-inspired propulsion and gyroscopic actuation with sensor modules distributed over the vehicle surface to provide unprecedented capabilities extending beyond the current influence of underwater robots. Within the scope of this research, I will advance hybrid class AUV instrumentation from the preliminary validation level to a

complete robust format, and perform the first in-water characterization. Figure 1 shows a mock-up of the proposed hybrid class vehicle architecture.

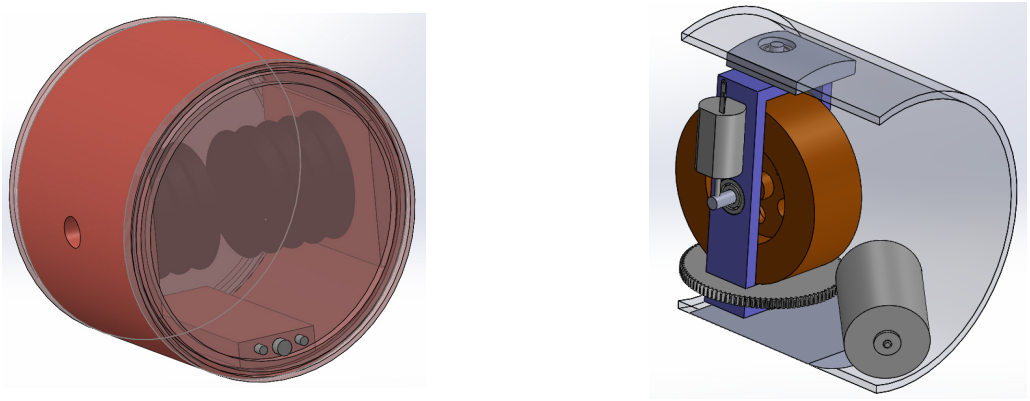

Figure 2: *Left*) Maneuvering thruster/actuation modules with cross-through connections, customizable nozzle, and internal cavities. *Right*) Control moment gyroscope module cut-away with flywheel, gimbal, and DC motors

This proposed hybrid-class vehicle concept will contain two operational modes: *AUV-mode* and *ROV-mode*. *AUV-mode* will be used for efficient travel in the forward surge direction, or for concepts of operation including surveying (e.g., "mowing the lawn") and/or reaching a particular area of interest. *ROV-mode* will instead use the coupled Control Moment Gyroscope (CMG) and thruster actuation modules in figure 2 to provide fine-tuned control inputs in all six degrees of freedom (DOF), enabling higher-accuracy low-speed maneuverability. In order to provide the underwater vehicle with the necessary abilities to operate in *ROV-mode*, research is divided into to the development of three distinct modules: the hydrodynamic sensor module, the thruster module, and the CMG module; with research and development efforts performed during the Link period of performance limited to the CMG and sensor modules in particular.

I.i.b Hydrodynamic Sensor Module

Unlike many existing underwater robots, marine life native to chaotic environments are capable of effectively navigating through turbulence. The combination of multimodal propulsion schemes and distributed sensing allows these organisms to adapt to a diverse set of environmental conditions [2]. Compared to standard error feedback control techniques, integrating a distributed array of environmental sensor modules over the vehicle body will enable a robot to directly measure fluid disturbances and account for them instantaneously. This technique

was demonstrated in [3] with an AUV in a laboratory tank, showing 72% improvement in positioning accuracy in the sway direction. An ocean-deployed system will encounter fluid disturbance forces in all directions and will experience significant viscous drag forces at higher speeds, requiring measurement of the shear stress distribution to accurately determine the total hydrodynamic forces in all 6-DOF. In addition to pressure distribution sensing demonstrated in [3], the enhanced sensor shell will add hot-film sensors to measure temperature and shear stress simultaneously.

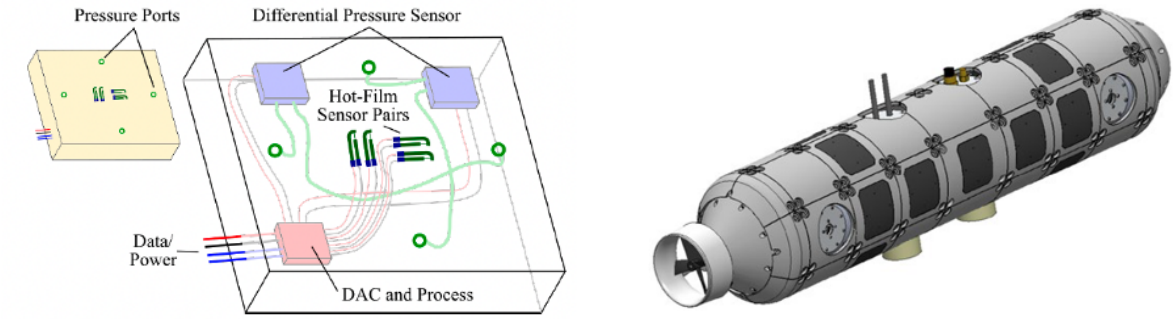

Figure 3: Proposed lateral line inspired modular sensor shell architecture. *Left*) Individual hydrodynamic sensor module schematic. *Right*) Complete modular sensor shell fit to AUV hull form [3]

Fluid surroundings have a significant impact on underwater vehicles due to the large fluid density and regular presence of waves and currents. Traditional sensing interprets fluid disturbances indirectly; whereby vehicle kinematics, determined from inertial measurements, are related to hydrodynamics through models assuming a steady state fluid, or fluid properties are measured by cumbersome, power intensive, and/or prohibitively expensive sensors (e.g., ADCP, DVL). I aim to develop a sensory system that provides instantaneous knowledge of an underwater robot's immediate surroundings by creating a hydrodynamic sensor module that measures both the pressure gradient and shear stress surrounding the vehicle hull form. Modules will be placed throughout the body surface, similar to the "lateral-line" sensory system observed in fish..

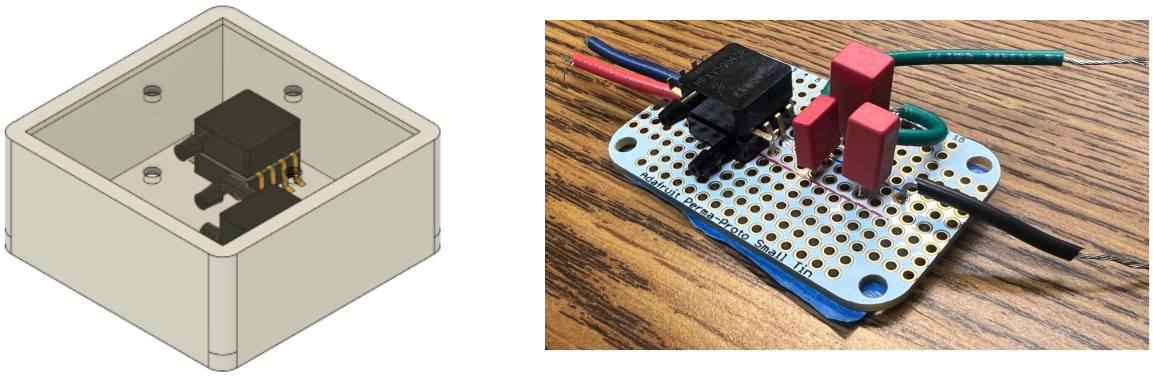

Figure 4: *Left*) Simplified 3-Dimensional Model of Hydrodynamic Sensor Module. *Right*) Solder Board Module Prototype

I.i.c Control Moment Gyroscope Module

Active roll control can generate complex body motions when combined with other vehicle actuation modes. Gyroscopic roll control actuators will be developed to enable unrestricted locomotion with the ability to position the vehicle thrusters to correct for fluid disturbance forces in both the heave and sway directions.

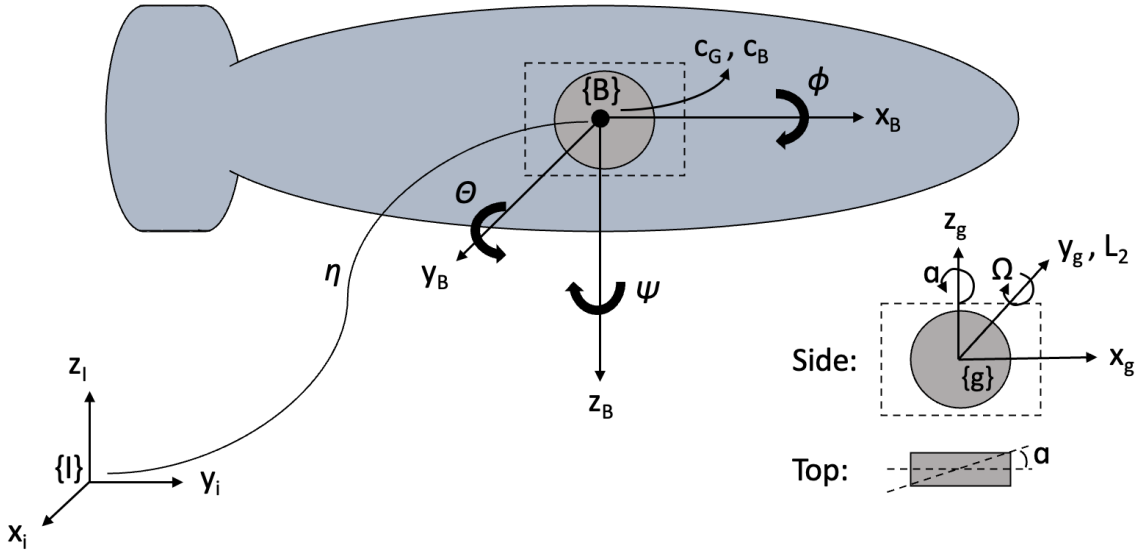

Figure 5: Single CMG Simulation Configuration

Figure 5 shows the Inertial coordinate frame {I}, the vehicle body-fixed coordinate frame {B}, and the CMG coordinate frame {g}.

I.ii Results

I.ii.a Hydrodynamic Sensor Module

In the realm of sensor technology, a balance exists between sensor range and accuracy. Extending a sensor's range, enabling it to detect signals across greater distances, is oftentimes desirable. However, as the range increases, accuracy tends to diminish. This trade-off is rooted in the challenges of capturing precise measurements across larger ranges, where factors such as signal attenuation and environmental noise become more influential. With any absolute gauge sensor, the sensing resolution becomes overly saturated at any appreciable water depth. Therefore, a differential pressure sensor, selected for high accuracy measurements based on an improved dynamic range compared to absolute gauge pressure sensors, was integrated with a breadboard prototype circuit to decouple the power supply and filter the data output via hardware. A LabView VI was developed for repeated calibration and filtering trials, including the most recent trials conducted with the prototype circuit in a lower profile solder board format.

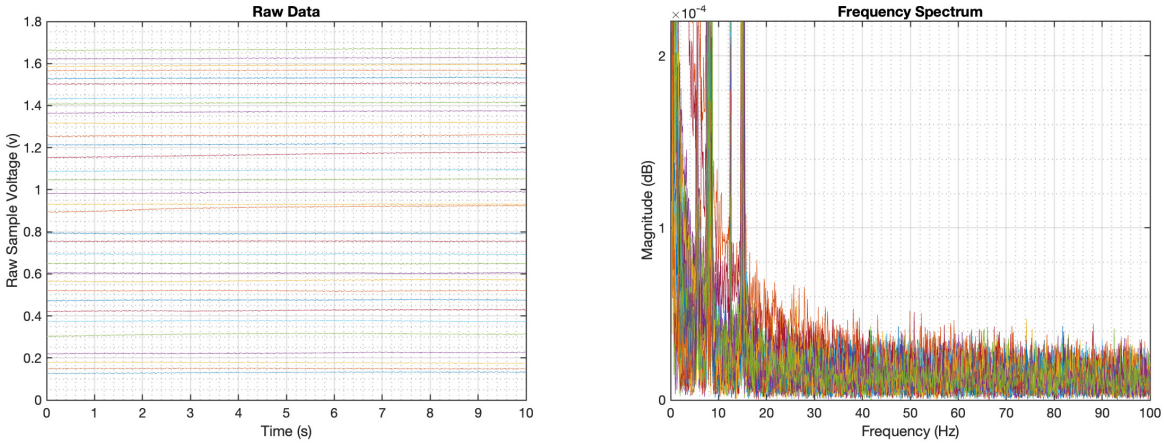

Figure 6: *Left*) Voltage samples over a 10s sample period, $f_s = 1$ kHz *Right*) Data frequency spectrum

A preliminary analysis of ocean wave spectra and predicted dynamic pressure signals provided a desired low-pass cutoff frequency to reduce sensor noise while still capturing all necessary dynamics. Numerous trials were conducted to determine appropriate components necessary to provide the desired ∼150 Hz cutoff frequency via filtering with hardware. An analysis was conducted which introduced high frequency noise into the the sample signal by placing the board on top of a high-frequency vacuum pump vibration source. Figure 7 shows

that with a Resistor-Capacitor (RC) Circuit implemented with values of 750 Ω and 1.5 μF respectively, a low-pass sampling cutoff frequency of around 150 Hz is achieved, as shown in (1). The final prototype circuit diagram can be seen in figure 8.

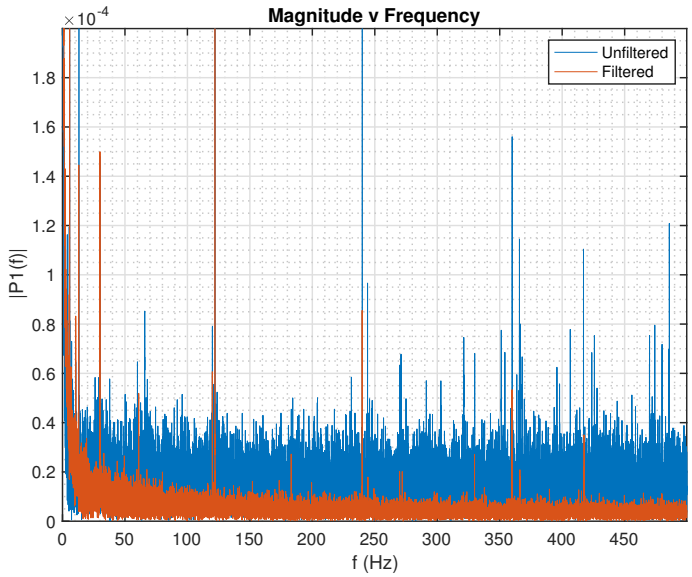

Figure 7: Spectral Analysis for High Frequency Vacuum Pump (RC Output Filter Circuit)

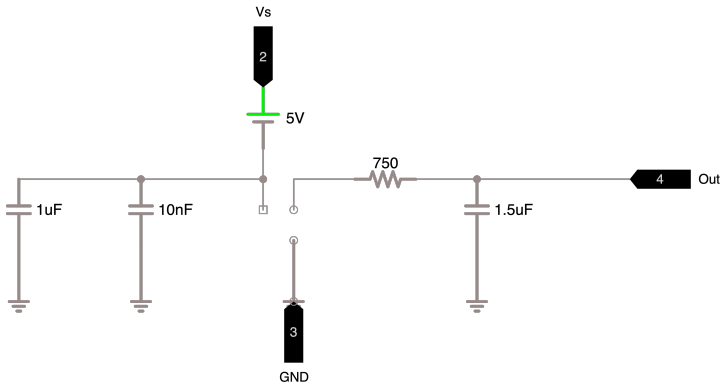

Figure 8: Integrated Pressure Sensor (IPS) Prototype Circuit

$$f_c = \frac{1}{2\pi RC} = \frac{1}{2\pi(750\Omega)(1.5x10^{-6}F)} = 141.47\text{Hz} \tag{1}$$

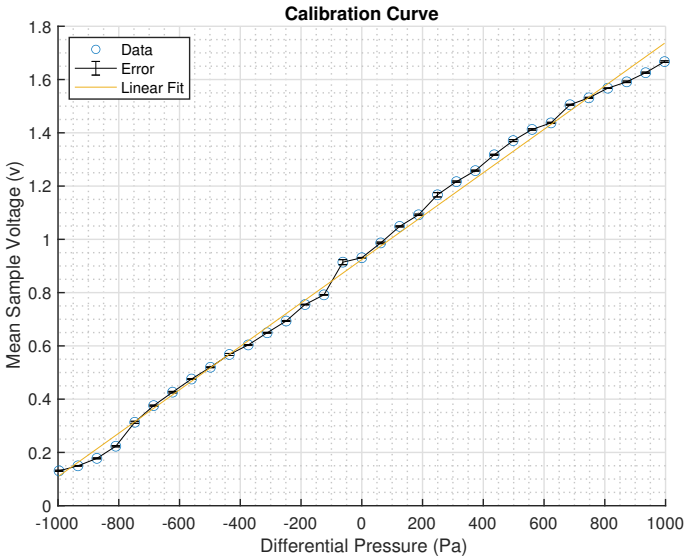

Figure 9: Mean Sample Voltage (v) vs. Differential Pressure (Pa). Error bars indicate RMS values of average values subtracted from raw data

Figure 9 shows the most recent calibration trial conducted for the differential pressure sensor. This plot compares the mean sample voltage measured at $f_s = 1$ kHz for a 10 second sample. The y-axis indicates the differential pressure measured between vinyl tubes connected to both ports of the sensor that were vertically separated and submerged in a small fish tank. A linear trend confirms the functionality of the sensor in an underwater environment, and underscores the necessity of meticulous calibration for each sensor. Calibration, involving precise adjustments to both slope and offset, is essential to align the sensor's output with actual measurements. The slope calibration fine-tunes scaling factors for proportional response to changes in the property being measured, while offset correction addresses inherent biases. These calibration procedures gain added significance due to the diverse factors impacting underwater environments, including pressure and temperature variations. Ultimately, a reliable linear relationship ensures accurate data capture, making calibrated sensors indispensable for consistent performance in dynamic underwater conditions.

I am currently prototyping with a Texas Instruments (TI) microcontroller (MCU) evaluation board to perform Analog/Digital Conversion (ADC) of the pressure signal at the module level, with an I2C parallel communication protocol implemented for querying data from the module(s). Work is being performed to create a custom software suite for ADC, memory allocation, and I2C communication between modules and a local machine. A custom Printed Circuit Board (PCB) is being designed in order to power the Integrated Pressure Sensor (IPS) as well as a pair of hot-film sensors utilizing a Constant Voltage (CV) application, driven at

5V and 10 mA. This PCB will also be designed around the TI ARM Cortex-M4 MCU chip to control sampling/sensing and serial communications.

I.ii.b Control Moment Gyroscope Module

This proposed system will utilize a combined roll/yaw control scheme, where the vehicle will roll to a desired angle before producing thrust forces in the body-fixed yaw plane via a jet propulsor payload developed in [1] and [2]. Thrust forces are generated by the periodic expansion and compression of the hull-internal thrust module cavity, with a small flow outlet on the vehicle side to minimize drag effects, allowing generation of desired control forces while maintaining a hydrodynamic profile for efficient forward travel. While attempting to use gyroscopes to control pitch or yaw motions is impractical due to the drag associated with such maneuvers, the low hydrodynamic forces associated with roll motions of radially symmetric vehicles make this an optimal solution. This unique actuation capability and the desire to create efficient 3D path following in a typical underactuated vehicle looks to bypass the loss of control authority with vehicles utilizing control surfaces.

Research is still in the proof of concept modeling and simulation phase. I designed and simulated an individual internal CMG for this hybrid-class control scheme to actively control the roll angle of the vehicle (see figure 5). For this proposed hybrid-class control scheme, an individual hull-internal CMG module is simulated to actively control the roll (ϕ) angle of the hybrid-class vehicle.

Considering standard SNAME notation for marine vehicles [4], and adopting the syntax of the inertial state vector $\boldsymbol{\eta}$, body-fixed state vector $\boldsymbol{\nu}$, and body-fixed force/torque vector $\boldsymbol{\tau}$ from [5], including conventional forms of vehicle position, orientation, body-fixed linear and angular velocities, forces, and torques:

$$\boldsymbol{\eta} = \begin{bmatrix} x \\ y \\ z \\ \phi \\ \theta \\ \psi \end{bmatrix} \quad ; \quad \boldsymbol{\nu} = \begin{bmatrix} u \\ v \\ w \\ p \\ q \\ r \end{bmatrix} \quad ; \quad \boldsymbol{\tau} = \begin{bmatrix} X \\ Y \\ Z \\ K \\ M \\ N \end{bmatrix} \tag{2}$$

In this form, $\boldsymbol{\eta}$ represents vehicle position in the inertial frame ($\boldsymbol{\eta_1} = [x, y, z]^T$) and orientation ($\boldsymbol{\eta_2} = [\phi, \theta, \psi]^T$), $\boldsymbol{\nu}$ represents vehicle linear ($\boldsymbol{\nu_1} = [u, v, w]^T$) and angular ($\boldsymbol{\nu_2} = [p, q, r]^T$)

velocities in the body-fixed frame, and $\boldsymbol{\tau}$ as body-fixed vehicle forces ($\boldsymbol{\tau_1} = [X, Y, Z]^T$) and torques ($\boldsymbol{\tau_2} = [K, M, N]^T$). Now considering the Rigid Body Rotational dynamics for an AUV with 6-DOF:

$$\boldsymbol{\tau} = \begin{bmatrix} X \\ Y \\ Z \\ K \\ M \\ N \end{bmatrix} = \begin{bmatrix} m(\dot{u} + qw - rv) \\ m(\dot{v} + ru - pw) \\ m(\dot{w} + pv - qu) \\ \dot{p}I_1 - qrI_2 + qrI_3 \\ \dot{q}I_2 + prI_1 - prI_3 \\ \dot{r}I_3 - pqI_1 + pqI_2 \end{bmatrix} \tag{3}$$

where τ consists of the equations modeling forces and torques in 6-DOF, assuming that the body-fixed coordinate system is fixed to the center of gravity and that the cross products of inertia are negligible. Considering the torque (moment) on the AUV as a function of the vehicle angular momentum $\boldsymbol{L_1}$:

$${}^B\boldsymbol{\tau_2} = \frac{\mathrm{d}}{\mathrm{d}t}\left({}^B\boldsymbol{L_1}\right) = \begin{bmatrix} K \\ M \\ N \end{bmatrix} \tag{4}$$

where $\boldsymbol{\tau_2}$ is equivalent to the vehicle body-fixed torques with respect to $\boldsymbol{L_1}$.

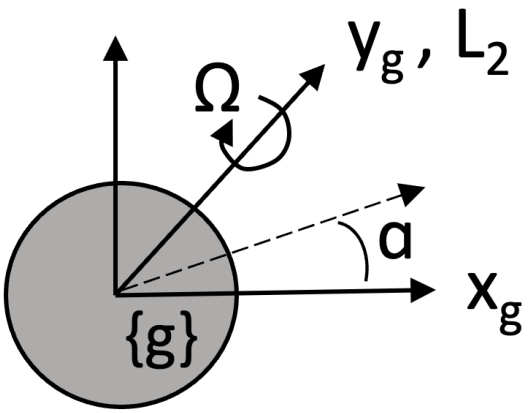

Figure 10: CMG Coordinate System {g}

A single CMG will be placed at point $C =< CG, CB >$ in order to simplify the rigid body rotational dynamics. The figure 5 cutaway, highlighted in the lower-right, as well as in

figure 10 shows the CMG flywheel angular velocity Ω, the angular momentum axis $\boldsymbol{L_2}$, and the CMG deflection angle α measured about z_g. In this particular configuration, the CMG consists of a uniform thin disc flywheel fixed in a gimbal system that allows the gyroscope coordinate frame {g} to rotate about the parallel vertical axes z_b and z_g, with α defined as the angle between x_b and x_g.

Considering the general expressions for angular momentum of a spinning flywheel,where $\boldsymbol{L}_2$ is the CMG angular momentum, I is the mass moment of inertia (with mass, m, and the square of the radius of gyration, r), and the flywheel angular velocity Ω:

$$ {}^{g}\boldsymbol{L}_2 = {}^{g}\, I\boldsymbol{\Omega} = {}^{g}\, I \begin{bmatrix} 0 \\ \Omega \\ 0 \end{bmatrix} = {}^{g}\, I\Omega \begin{bmatrix} 0 \\ 1 \\ 0 \end{bmatrix} \quad ; \quad {}^{g}I = \frac{1}{2}mr^2 \tag{5} $$

Newton's second law states that the angular acceleration is proportional to the net torque and inversely proportional to the moment of inertia. While the conservation of angular momentum can only be explicitly applied in the inertial frame, it is more convenient to define linear and angular velocities in the body-fixed frame. Defining a rotation matrix to transform between coordinate frames {B} and {g}, with ${}^{B}_{g}R$ describing frame {g} relative to and defined in frame {B}, we can pre-multiply the CMG angular momentum ${}^{g}\boldsymbol{L_2}$ to transform into the body-fixed coordinate system:

$$ {}^{B}\boldsymbol{L_2} = {}^{B}_{g}\, R {}^{g}\boldsymbol{L_2} = \begin{bmatrix} c(\alpha) & -s(\alpha) & 0 \\ -s(\alpha) & c(\alpha) & 0 \\ 0 & 0 & 1 \end{bmatrix} \begin{bmatrix} 0 \\ {}^{g}I\Omega \\ 0 \end{bmatrix} = {}^{g}\, I\Omega \begin{bmatrix} -s(\alpha) \\ -c(\alpha) \\ 0 \end{bmatrix} \tag{6} $$

With the CMG angular momentum $\boldsymbol{L_2}$ defined in the body-fixed coordinate frame {B}, we can now define the body-fixed torques as a function of CMG angular momentum:

$$ {}^{B}\boldsymbol{\tau}_{cmg} = \begin{bmatrix} K \\ M \\ N \end{bmatrix} = \frac{\mathrm{d}}{\mathrm{d}t}\left({}^{B}\boldsymbol{L_2}\right) + {}^{B}_{I}\,\boldsymbol{\omega}_B \times {}^{B}\,\boldsymbol{L_2} = \frac{\mathrm{d}}{\mathrm{d}t}\left({}^{B}\boldsymbol{L_2}\right) + \begin{bmatrix} p \\ q \\ r \end{bmatrix} \times {}^{g}\, I\Omega \begin{bmatrix} -s(\alpha) \\ -c(\alpha) \\ 0 \end{bmatrix} \tag{7} $$

The second and third terms in (7) are easily defined. The first term is determined by taking the time derivative of the gyroscope angular momentum ${}^{g}\boldsymbol{L_2}$, and transforming the expression into the body-fixed vehicle frame using rotation matrix ${}^{B}_{g}R$:

$$\frac{\mathrm{d}}{\mathrm{d}t}\left({}^{B}\boldsymbol{L_2}\right) = {}^{B}_{g}R\left(\frac{\mathrm{d}}{\mathrm{d}t}\left({}^{g}\boldsymbol{L_2}\right) + {}^{g}_{B}\boldsymbol{\omega}_g \times {}^{g}\boldsymbol{L_2}\right) =$$

$$ {}^{B}_{g}R\left({}^{g}I\dot{\Omega}\begin{bmatrix}0\\1\\0\end{bmatrix} + \begin{bmatrix}0\\0\\\dot{\alpha}\end{bmatrix} \times {}^{g}I\Omega\begin{bmatrix}0\\1\\0\end{bmatrix}\right) = \begin{bmatrix} c(\alpha) & -s(\alpha) & 0\\ -s(\alpha) & c(\alpha) & 0\\ 0 & 0 & 1\end{bmatrix}\begin{bmatrix}-{}^{g}I\Omega\dot{\alpha}\\ {}^{g}I\dot{\Omega}\\ 0\end{bmatrix} =$$

$$\begin{bmatrix}-c(\alpha){}^{g}I\Omega\dot{\alpha} - s(\alpha){}^{g}I\dot{\Omega}\\ -s(\alpha){}^{g}I\Omega\dot{\alpha} - c(\alpha){}^{g}I\dot{\Omega}\\ 0\end{bmatrix} \quad (8)$$

Plugging in the expression for $\frac{\mathrm{d}}{\mathrm{d}t}\left({}^{B}\boldsymbol{L_2}\right)$ back into (7) and performing the cross product between the second and third terms yields the body-fixed torque induced by the CMG:

$$\boxed{{}^{B}\boldsymbol{\tau}_{cmg} = \begin{bmatrix}-c(\alpha){}^{g}I\Omega\dot{\alpha} - s(\alpha){}^{g}I\dot{\Omega} - {}^{g}I\Omega c(\alpha)r\\ -s(\alpha){}^{g}I\Omega\dot{\alpha} - c(\alpha){}^{g}I\dot{\Omega} - {}^{g}I\Omega s(\alpha)r\\ {}^{g}I\Omega(s(\alpha)q - c(\alpha)p)\end{bmatrix}} \quad (9)$$

This simulation case study will help to determine the feasibility of a single CMG roll control maneuvering scheme, starting with a simulated fully submerged vehicle at rest attempting to roll $+90°$ within a control cycle. Additionally, the analysis of sensitivity stability plots will aid in the mechanical design process for a physical CMG payload module, while also providing a virtual environment to investigate the interactions of $\boldsymbol{\nu_2}$ terms on the CMG roll control dynamics. This dynamic simulation suite considers a fully submerged AUV performing CMG-based active roll control throughout a variety of body motions. This simulation helps lay the foundation of a reasonable proof of concept, testing desired roll angle convergence within a single vehicle control cycle. By including actuator dynamics and limitations within the vehicle simulation, results will help drive necessary design choices for the mechanical design of the CMG module, including necessary motor torques for the flyhweel and gimbal systems and gear ratios required to provide the proper amount of inertia.

The CMG module is limited by a small diameter and limited power. This simulation case study provides the necessary framework in order to determine critical design features of the CMG module, guaranteeing that the DC motors inside the module are specified to provide necessary CMG torque actuation. Motion of the underwater vehicle is simulated in Matlab by integrating vehicle dynamics (10) over time through a set of ancillary functions in order

to converge to a desired roll-angle in a single control cycle. The functions necessary for simulation included a controller code, a code to calculate CMG body-fixed torques based on (9), and a vehicle dynamics code. Given a set of control forces acting on the vehicle $\tau_c = [X, Y, Z, K, M, N]^T$. the body-fixed acceleration is governed by the dynamic equation from [5]:

$$\tau_c = [M_{RB} + M_A]\,\dot{\nu} + [C_{RB} + C_A + D]\,\nu \tag{10}$$

where M_{RB} is the rigid-body mass/inertia matrix, C_{RB} is the rigid-body centripetal/Coriolis matrix , M_A and C_A are the added mass and centripetal/Coriolis matrices respectively, and D is the drag matrix.

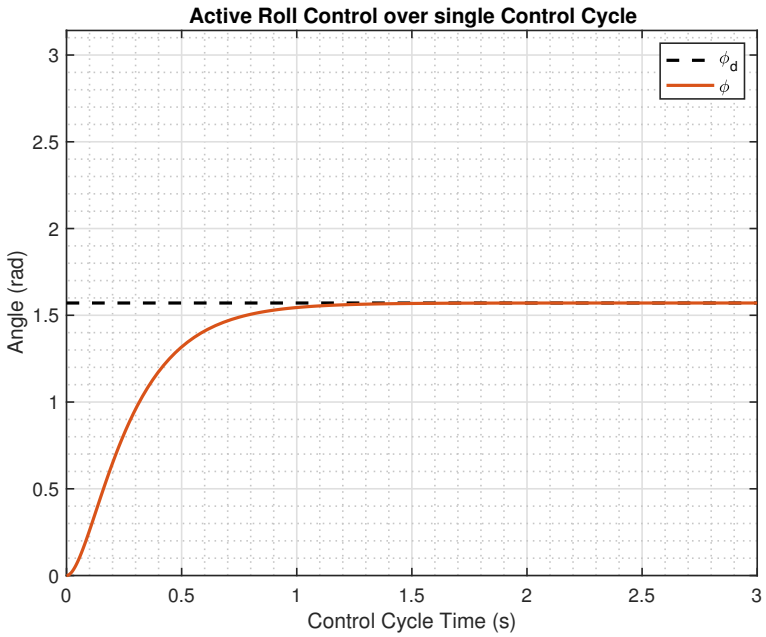

Figure 11: Vehicle roll angle over single control cycle of 3 s. Vehicle starts from rest and actively rolls to 90°

Certain issues arising with the current simulation suite are in troubleshooting, and create motivation for including an additional CMG module in future simulations. In order to improve simulation results, a continued simulation case study will move to a dual CMG configuration. Starting with a new governing equation derivation that moves away from a single CMG module placed at the center of gravity, and moving to 2 CMGs placed aft and forward respectively (as observed in figure 1). This derivation will also account for physics associated with linear forces produced by torques generated away from the center of gravity

as well as the inclusion of parallel axis theorem. This improved simulation suite will aid in the development of the CMG roll control actuator mechanical design as well, assisting in the definition of necessary motor torques for flywheel and gimbal systems, and required gear ratios required to generate necessary amounts of inertia.

I.iii Significance and Impact

This novel approach to enhance robot performance seeks to evolve conventional methods for robotic sensing and control theory from an overly centralized process requiring numerous assumptions to an instinctive process emphasizing improved perception and navigation of local fluid surroundings. An innovative robotic automation methodology which simplifies or circumvents complex nonlinear models of fluid-body interactions represents a fundamentally different approach to marine robot technology. Coupling non-conventional bio-inspired propulsion/maneuvering with novel control algorithms which improve position tracking accuracy will result in a hybrid class AUV capable of efficiently traversing long distances without sacrificing low speed high-accuracy maneuvering. Environmental awareness provided to the AUV will result in unprecedented locomotion control, revolutionizing current concept of operations for autonomous underwater systems. Novel applications include improved search and rescue methods, capable of efficiently examining underwater wreckage sites too dangerous for human operators. High accuracy position tracking at low speeds makes this hybrid class AUV ideal for a permanent underwater presence, capable of docking with underwater power and data stations for persistent missions such as waterside security, cable and pipeline inspection, and data collection. Distributed sensing of local fluid surroundings allows for improved detection of fluid body/structure interactions, enabling use in hazardous areas such as chaotic littoral zones, confined channels, and shallow reef areas. Research will also greatly aid efforts towards higher accuracy control of underwater soft robotics, where fluid body interaction modeling over an entire operational envelope is a significant challenge. Knowledge gained from data collection in these dynamic, information-rich ocean regions will have a transformative impact on oceanographic sampling and measurement techniques, leading to improved modeling and simulation seeking to better understand and combat phenomena like climate change and resulting sea level rise.

I.iv Where might this lead?

This work will lead to the continued development of a new suite of hybrid class vehicles utilized by both academic and defense research communities. By combining design aspects; including sensing methodologies, actuation/propulsion modes, and/or the marriage of design concepts between vehicles classes - a new regime of underwater vehicles with improved actuation and robust sensing techniques will aid undersea research efforts for decades to come.

References

[1] M. Krieg, K. Nelson, J. Eisele, and K. Mohseni, "Bioinspired jet propulsion for disturbance rejection of marine robots," *IEEE Robotics and Automation Letters*, vol. 3, no. 3, pp. 2378–2385, 2018. [Online]. Available: http://dx.doi.org/10.1109/LRA.2018.2812219

[2] J. C. Liao, "A review of fish swimming mechanics and behaviour in altered flows," *Philosophical Transactions of the Royal Society B*, vol. 362, no. 148, pp. 1973–1993, 2007. [Online]. Available: http://dx.doi.org/10.1098/rstb.2007.2082

[3] M. Krieg, K. Nelson, and K. Mohseni, "Distributed sensing for fluid disturbance compensation and motion control of intelligent robots," *Nat. Mach. Intell.*, vol. 1, pp. 216–224, 2019. [Online]. Available: https://doi.org/10.1038/s42256-019-0044-1

[4] SNAME, "Nomenclature for treating the motion of a submerged body through a fluid," Society of Naval Architects and Marine Engineers, New York, USA, Tech. Rep. Technical Report Bulletin 1-5, 1950.

[5] T. I. Fossen, *Guidance and Control of Ocean Vehicles*. Hoboken, NJ, USA: Wiley-Interscience, 1994.

II Journal Papers & Scholarly Reports

Pending additional instrumentation and simulation research and development efforts, two papers are planned for submission in Fall 2023:

- T.J. Inkley, M. Krieg. Dynamic Simulation of Autonomous Underwater Vehicle Active Gyroscopic Roll Control. *Paper in Progress*
- T.J. Inkley, M. Krieg. A Hydrodynamic Sensor Module for Improved Underwater Vehicle Perception. *Paper in Progress*

III Fellowship Impact

Being selected for the Link Foundation Ocean Engineering and Instrumentation Fellowship has set me on a path of continued exposure to novel and interesting aspects of underwater technology. After pivoting away from an ocean engineering research focus on wave modeling and simulation of hurricane and and tsuanmigenic events, this fellowship has exposed me to underwater instrumentation topics I was unaware of, and has supplemented my interest in developing technology capable of investigating deep, dark, and dynamic ocean regions where the current state of the art struggles to perform. By actively performing research and development efforts working towards combining the most beneficial design aspects of AUVs and ROVs, I have been exposed to a suite of underwater vehicles I previously had very little knowledge about. The Link Fellowship has helped to cement my decision to continue pursuing my quest for knowledge surrounding areas of our planet's oceans where we still posses a very limited understanding.